Triclinic $LiVPO_4F/C$ cathode for aqueous rechargeable lithium-ion batteries

Rangaswamy Puttaswamy[1, 2], Suresh Gurukar Shivappa[1]*, Mahadevan Kittappa Malavalli[2], Yanjerappa Arthoba Nayaka[3]

[1]*Department of Chemistry and Research Center, N.M.K.R.V. College for Women, Jayanagar, Bangalore 560011, India*
[2]*PG-Center, Kuvempu University, Kadur 577548, Karnataka, India*
[3]*Department of Chemistry, School of Chemical Science, Kuvempu University, Shankaraghatta, Shimoga 577451, Karnataka, India*

*Corresponding author: Tel: (91) 80-22443695; E-mail: sureshssmrv@yahoo.co.in

DOI: 10.5185/amlett.2019.2141
www.vbripress.com/aml

Abstract

Triclinic $LiVPO_4F/C$ composite material is synthesized by Reaction under autogenic pressure at elevated temperature (RAPET) method and for the first time, we have evaluated the electrochemical properties and performance in aqueous electrolyte. Structural and morphological features of the material have been characterized using X-ray diffraction and scanning electron microscopy techniques. The electrochemical properties and performance of the material has been evaluated by using cyclic voltammetry, galvanostatic charge/discharge studies, electrochemical impedance spectroscopic technique and potentiostatic intermittent titration technique. The complete electrochemical studies of $LiVPO_4F/C$ composite material have been performed in 0.1M Li_2NO_3 with 0.05 mL glycerine as an additive in 10 mL of H_2O as an aqueous electrolyte and its working mechanism was described using standard three-electrodes as well as two electrode configurations. Copyright © 2019 VBRI Press.

Keywords: Aqueous electrolyte, $LiVPO_4F/C$, $LiTiPO_4F$, RAPET, electrochemical studies.

Introduction

Even though many advances have been achieved in conventional rechargeable lithium-ion battery systems, still it is a challenging task for the researchers to find new approaches for the synthesis of electrode materials and to improve the electrochemical properties such as capacity, stability, and conductivity with low cost. Fluorophosphate based electrode materials have been gain tremendous interest from past two decades, due to their good electrochemical properties and performances such as higher energy density, good reversibility and stable cycle life, high operating potential and thermal stability [**1-3**]. Up to date, several fluorophosphate cathodes have been studied, which mainly including $LiVPO_4F$ [**4, 5**], $LiCoPO_4F$ [**6**] $LiTiPO_4F$ [**7, 8**] etc. Among them, $LiVPO_4F$ is one of the most promising high voltage cathode material for non-aqueous rechargeable lithium-ion battery applications [**5, 9-11**]. The physico-electrochemical properties of $LiVPO_4F$ electrode have been studied by several research groups in detail both theoretically and experimentally for the applications in non-aqueous rechargeable Li-ion battery systems [**4, 12**]. The combination of the stronger inductive effect of PO_4^{3-} anion with fluorine plays an important role in the enhancement of working electrode potential of about 4.2 V vs. Li^+/Li based on V^{3+}/V^{4+} redox couple [**1**]. Usually, $LiVPO_4F/C$ electrode material has been synthesized by two-step solid-state/ceramic methods. VPO_4 formed as an intermediate product which requires high temperature for a long time [**10**] and the poor rate performance of this material is hindered its further development as the next generation commercial cathode material. A high-temperature carbothermal methods [**13**] and sol-gel [**4**] methods were also employed to synthesize $LiVPO_4F$ and $LiVPO_4F/C$ at high temperature for a longer period of time and the capacity and cycling life are limited to only a few cycles. To solve the aforementioned problems, significant research efforts have been focused on the development of simple, low cost, less time consuming and low-temperature synthesis for large-scale productions. RAPET method, which was first proposed by Pol *et al.* [**14**] is a low-temperature approach applied for the synthesis of micro and nano-sized metals, metal oxides and metal sulfides etc, this method has several advantages over existing high-temperature solid-state methods [**3**]. It consists of simple calcination procedure by employing Swagelok cell reactor to maintain the reactants with high pressure and the moderate temperature inside the tubular furnace [**3**].

Aqueous rechargeable lithium-ion battery system was first proposed by Dahn and co-workers [**15**] is one of the best, simple, cost-effective, and promising alternatives for safer lithium-ion battery applications [**3**]. From the aqueous electrolyte, it is possible to resolve the several challenges associated with non-

aqueous electrolyte. The use of aqueous electrolyte is not only resolved the safety problems but also offer several advantages such as, easy cell assembly, eco-friendliness, low toxicity etc. [**16**]. Although, low capacity of electrode materials in aqueous electrolytes they exhibited stable cycle life more than that of a non-aqueous electrolyte counterpart [**17**] and the capacity achieved by some aqueous rechargeable battery systems are higher than the Ni-Cd (40-50 mA h g^{-1}) battery system. In addition to the above advantages, from the aqueous rechargeable battery systems, it can be possible to reach the capacity level of Ni-MH battery system (~200 mA h g^{-1}) by further improvements [**18**] with latest technologies. However, in order to overcome issues related with low conductivity, capacity and stability of the electrode materials in non-aqueous electrolytes, some research groups enhanced the electrochemical properties and performance of some electrode materials by adding organic additives to the electrolytes [**19, 20**].

Considering the above facts, herein we are reporting the simple synthesis strategy called RAPET method to prepare triclinic $LiVPO_4F$/C electrode material. The product obtained was subjected to physical and electrochemical characterizations. In this regard, we have studied and analyzed the electrochemical properties of $LiVPO_4F$/C using glycine as an organic additive in 0.1 M Li_2NO_3 aqueous electrolyte to improve the electrochemical properties of $LiVPO_4F$/C cathode for the first time. The cell performance and electrochemical activities were studied by using cyclic voltammetry (CV), galvanostatic charge/discharge cycling, electrochemical impedance spectroscopy (EIS) and potentiostatic intermittent titration technique (PITT). Galvanostatic charge/discharge studies of $LiVPO_4F$/C were studied by the combination of $LiVPO_4F$/C cathode and $LiTiPO_4F$ anode material [**3, 8**]. The electrochemical properties of $LiVPO_4F$/C in aqueous rechargeable lithium-ion battery have not yet been reported to the best of our knowledge.

Experimental

Material synthesis

Triclinic $LiVPO_4F$/C was synthesized by using V_2O_5, $NH_4H_2PO_4$, carbon black and LiF as starting precursor's materials. Whereas, TiF_3, $NH_4H_2PO_4$, LiOH and carbon black were used for the synthesis of $LiTiPO_4F$ anode material. All chemicals were purchased from Sigma-Aldrich and pure water was used throughout the experiments.

In a typical synthesis procedure, stoichiometric amounts of V_2O_5, $NH_4H_2PO_4$, and carbon black were blended manually for 30 min and pressed into pellets for uniform distribution. The mixed precursor was introduced into the 5 mL capacity Swagelok reactor, made up of stainless steel, close tightly by two caps from both sides in an Argon atmosphere and placed inside the tubular furnace. The precursors inside Swagelok reactor was maintained at 500 °C for the optimized time of 3h. The intermediate product VPO_4 was formed [**4**], which was cooled to room temperature and again ground well with stoichiometric amounts of LiF (20 wt% extra is added to complete conversion) and finally transferred again into a tubular furnace at 500 °C for 4h at a rate of 10 °C/min by flowing Ar gas. The final product was cooled to room temperature and used for aqueous battery applications.

$LiTiPO_4F$/C anode material was also prepared by RAPET method [**3**]. In this scheme, the synthesis of $LiTiPO_4F$/C was carried out in a single step procedure. Stoichiometric amounts of $NH_4H_2PO_4$, LiOH, TiF_3 and carbon black were mixed and ground well for 20 min into a fine powder in an Ar atmosphere. After proper mixing the precursors were introduced into the 5 mL capacity Swagelok stainless steel reactor and placed in the middle of the tubular furnace at 600 °C for 15h. The heating and cooling rate was 10 °C/min. The $LiTiPO_4F$/C product was used as an anode which was combined with $LiVPO_4F$/C cathode for galvanostatic charge/discharge studies.

Material characterization and cell assembly

Structure of the products were characterized by XRD Benchtop powder diffraction system with CuKα source (λ=1.5418 °A). Scanning electron microscopy (Zeisf Model Supra, Germany) was used to observe the surface characterization of the products. Electrodes for aqueous rechargeable lithium-ion battery were prepared by using stainless steel mesh as a current collector. The mesh which was acts as a current collector was cut into the circular shape of about 0.5 mm in diameter and welded with stainless steel wire for electrical contact. The mesh was sandblasted to remove the oxide layer, washed with pure water, sonicated with acetone, dried and finally note down the weight before loading the sample. The preparation of both $LiVPO_4F$/C and $LiTiPO_4F$/C electrodes were conducted in a similar way. Powders samples of $LiVPO_4F$/C or $LiTiPO_4F$/C, carbon black powder and polyvinylidene fluoride were taken in the weight ratio of 75:15:10 in a mortar, ground well and the mixture was dispersed in N-methyl pyrrolidine solvent. The obtained slurry was stirred for 2h and uniformly coated onto the pre-treated stainless-steel mesh current collector. Vacuum dried at 80-100 ºC for 12h and note down the weight after drying. The electrochemical cells were assembled in a glass cell of 20 mL capacity containing 10 mL of aqueous electrolyte. The cell assembly of the $LiTiPO_4F$ anode was similar to that of $LiVPO_4F$/C cathode material.

The assembly of the cell consists of three-electrodes and two-electrode configurations. Three electrode electrochemical cells were used for CV, EIS, PITT and GITT measurements, it consists of saturated calomel electrode and pt wire electrode was used as a reference and counter electrodes, respectively. For two electrode systems, $LiVPO_4F$/C (cathode) was coupled with $LiTiPO_4F$/C (anode) and it was applied to galvanostatic charge/discharge experiments. Electrochemical impedance measurements were carried

out potentiometrically by applying AC excitation signal in the frequency range from 100 KHz to 5 MHz. PITT measurements were carried out at different potential steps. In PITT, sequences of potentiostatic steps were applied followed by pre-conditioning time (typically 600s) with 1h relaxation after each equilibrium potentials. There are 20 titrations points covering the whole discharge potentials range and the measurements were as small as 20 mV near the CV peak potentials. All the electrochemical measurements were performed at room temperature using a biologic potentiostat-galvanostat electrochemical workstation.

Results and discussion

Physical characterization

The powder X-ray diffraction pattern in **Fig. 1(a)** confirms the formation of crystalline product in triclinic form. $LiVPO_4F$/C particles have sharper peaks with an increased intensity which indicates that the pure crystals were obtained by RAPET method at low temperature with high pressure and the obtained patterns are well agree with those of the reported results [**12, 21**]. The 20% excessive LiF is added during the synthesis in order to compensate the loss of lithium and fluorine. There were no obvious impurity phases were observed in the sample. Similarly, phase purity of the $LiTiPO_4F$ was analyzed by powder X-ray diffraction studies. As shown in **Fig. 1(b)**, most of the diffraction peaks are sharper with increased intensity and the diffraction peaks are indexed to tavorite type structure [**22**] and this is well consistent with the reported article [**7**]. The very sharp peaks indicate the high degree of crystallinity and good electrochemical activity in terms of capacity and rate of lithium ion intercalation/de-intercalation. SEM micrographs of $LiVPO_4F$/C and $LiTiPO_4F$ electrode material are shown in the inset of **Fig. 1(a, b)** respectively. The particles of $LiVPO_4F$/C are non-spherical in shape with an average size of 300 to 500 nm. The well-aggregated particles are the result of the reaction, which takes place at an autogenic pressure at an elevated temperature that reduces the synthesis time and shortens the particle size. Such kind of morphology is very important to obtain both high specific capacity and good cycling stability. The SEM image of $LiTiPO_4F$ material have presented the irregular shapes with average sizes ranging from few hundred of nanometres to several micrometers-sized particles and particles distribution are less than 1 μm.

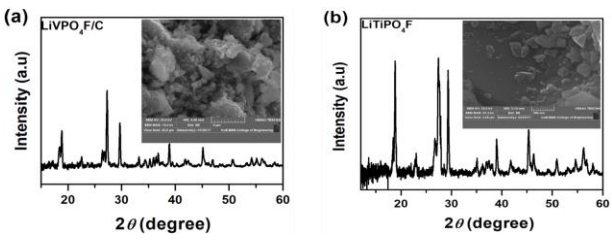

Fig. 1. XRD patterns of (a) $LiVPO_4F$/C cathode (b) $LiTiPO_4F$ anode materials synthesized by RAPET method (Inset: Corresponding SEM micrographs $LiVPO_4F$/C and $LiTiPO_4F$ electrode materials).

Electrochemical characterization

Cyclic voltammetry measurement

The stability of the electrode in aqueous as well as in non-aqueous electrolyte within the safe potential window is necessary due to the possibility of oxygen and hydrogen evolution in aqueous electrolyte and electrolyte degradation in case of the non-aqueous electrolyte. The analysis of peak current in different aqueous electrolyte was carried out; unfortunately, the absence of peak was observed for different lithium salts of the aqueous electrolytes. Finally, we succeeded with 0.1M Li_2NO_3 with 0.05 mL glycerin as an additive in 10 mL of water.

Fig. 2(a) shows the CV profile of $LiVPO_4F$/C with different aqueous electrolytes with 0.05 mL glycerine as a common additive at 0.05 mV s^{-1} scan rate. It can be seen that the CV profiles of $LiVPO_4F$/C changes with the type of electrolyte solutions. As can be seen from **Fig. 2(a)**, a good reversible peak with sharp redox peaks were achieved in 0.1M Li_2NO_3 with 0.05 mL glycerine aqueous electrolyte as compared to the CV obtained by LiOH and Li_2SO_4 aqueous electrolytes. In addition to these, the potential gap between the redox peaks is very small for Li_2NO_3 as compared to 0.1M LiOH and Li_2SO_4 electrolytes. This shows that, $LiVPO_4F$/C performs better electrochemical activities in the 0.1M Li_2NO_3 aqueous electrolyte.

Fig. 2(b) shows the cyclic voltammogram of $LiVPO_4F$/C electrode from 0.0 to 1.0 V vs. SCE at 0.05 mV s^{-1} scan rate. The CV exhibited one anodic/cathodic peak at 0.95/0.80 V. These peaks are corresponding to one Li^+-ions de-intercalation/ intercalation from/to $LiVPO_4F$/C electrode respectively. The well distinct current peaks in the CV indicate the good reversibility and better reactivity of $LiVPO_4F$/C in aqueous electrolyte. No evolution of oxygen and hydrogen was observed during intercalation/de-intercalation reactions in the potential range from -0.5 to +0.8 V. From the CV it is suggested that good reversibility and sharp redox peaks indicating the feasible electrode kinetics occurring in the 0.1M Li_2NO_3 aqueous electrolyte.

In order to confirm the absence of peak current from 0.05 mL glycerin as an additive, we run the CV with bare SS mesh current collector with 0.05 mL glycerin and 0.1M Li_2NO_3 as the aqueous electrolyte. No detectable peak currents were observed for this electrolyte in CV. The potential range is shown in **Fig. 2(b)** is classified into six potential domains. Totally there are six potential domains were classified for the cyclic voltammogram. Three potential domains for forwarding scan and remaining three potential domains for the reverse scan. During forward scan, the potential range is classified into three domains i.e. before de-intercalation of Li-ions, during de-intercalation of Li-ions and after de-intercalation of Li-ions represented by I, II and III respectively. Potential domain I, which indicates the region before de-intercalation of Li-ions, Potential domain II shows

the region during the de-intercalation of Li-ions and Potential domain III refers the complete delithiated state ($Li_{(1-x)}VPO_4F$). Similarly, for intercalation process, the potential range is also divided into three domains i.e. before intercalation of Li-ions, during intercalation of Li-ions and complete intercalation of Li-ions and they were indicated by I*, II* and III*.

Fig. 2(c) shows the typical cyclic voltammogram of $LiTiPO_4F$ anode in 2M Li_2NO_3 aqueous electrolyte at 0.05 mV s^{-1} scan rate in the voltage range from -0.8 to 0.5 V. The cyclic voltammogram shows that two pairs of redox peaks centered at negative potential region and it gives two distinct oxidation and one reduction peaks at -0.12/-0.16 V and -0.39/-0.55 vs. SCE corresponds to Li-ion de-intercalation and intercalation in $LiTiPO_4F$ respectively. Among them, one pair of redox peaks are due to the oxidation of Ti^{3+} to Ti^{4+} and for reduction of Ti^{4+} to Ti^{3+} with the corresponding Li^+-ion de-intercalation/intercalation. Another pair of redox peaks are pseudo peaks at equal amplitude [**22, 3**]. Hence, from the CV, it is clear that $LiTiPO_4F$ is considered as anode [**3**] material in the aqueous electrolyte.

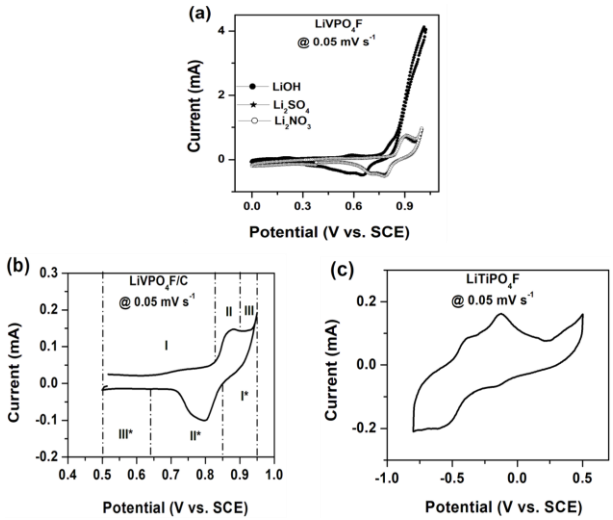

Fig. 2. (a) Cyclic voltammogram of $LiVPO_4F/C$ in 0.1M Li_2NO_3, Li_2SO_4, and LiOH with 0.05 mL glycerin as an additive (b) $LiVPO_4F/C$ in 0.1M Li_2NO_3 solution with 0.05 mL glycerine and (c) $LiTiPO_4F$ anode material in 2M Li_2NO_3 aqueous electrolyte at 0.05 mV s^{-1} scan rate.

Galvanostatic charge-discharge cycling

To further emphasize the electrochemical performance of the $LiVPO_4F/C$ material in the Li_2NO_3 aqueous electrolyte, the galvanostatic charge/discharge studies were carried out by using $LiVPO_4F/C$ cathode and $LiTiPO_4F$ as an anode **[Fig. 3(a)]**. Based on the CV results of both cathode and anode, the potential window was limited to -1 to +1 V. In particular, the $LiVPO_4F/C$ delivered 113 mA h g^{-1} for the first cycle at the C/2 (0.5 C) rate. Good reversible capacities were achieved except first discharge cycle. The cyclability of the battery cell is affected by the properties of both cathode, anode, and electrolyte. The cell performance of $LiVPO_4F/C$ in combination with $LiTiPO_4F$ has carried out up to 200 cycles at C/2 (0.5 C) rate is as shown in **Fig. 3(b)**. A steady-state decrease in the capacity was observed up to 200 cycles, this may be due to the dissolution of vanadium in electrolytes and decomposition of water [**24**]. In case of the 200th cycle, the cell delivers a reversible discharge capacity of 46 $mAhg^{-1}$. The columbic efficiency maintains almost stable (more than 90%), which shows good electrode efficiency in aqueous electrolytes. Although, steady-state decrease in the capacity by this combination in an aqueous electrolyte, but it illustrates the much better rate performance as compared to non-aqueous counterpart [**5**, **10, 12, 25**]. Hence, $LiVPO_4F/C$ cathode offers a good reversible de-intercalation and intercalation of lithium ions in the aqueous electrolyte (with the glycerine as an additive).

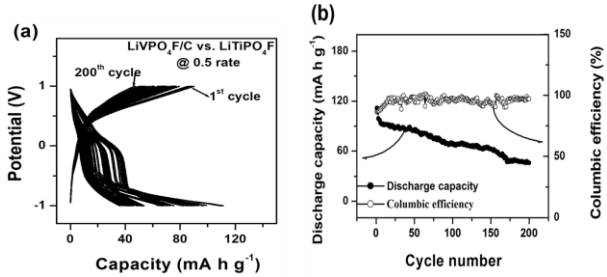

Fig. 3. (a) Galvanostatic charge/discharge measurements for $LiVPO_4F/C$ cathode combined with the $LiTiPO_4F$ anode at C/2 (0.5 C) rate and (b) Discharge capacity and columbic efficiency vs. number of cycles.

Potentiostatic electrochemical impedance spectroscopy studies

To understand the beneficial effects of 0.1M Li_2SO_4 aqueous electrolyte on the electrochemical performance of $LiVPO_4F/C$, we have studied the electrochemical impedance spectra for both charge and discharge process. EIS as a non-transient technique which does not alter the electrode-interface which make this technique more precise than CV studies. Before measuring the EIS, the electrodes were cycled for 3 to 4 cycles to stabilize the electrode. EIS in the aqueous electrolyte was carried out in the frequency range from 100 KHz to 5 MHz with AC modulation amplitude of 10 mV. The Nyquist plots obtained in 0.1M Li_2NO_3 aqueous electrolyte for both de-lithiated and lithiated process is differentiated into three potential domains according to CV potential domains.

Fig. 4(a-c) illustrates the typical Nyquist plots of the de-lithiation process measured at electrode potential range from of 0.5 to 1 V. The Nyquist plots of $LiVPO_4F/C$ electrodes included by major three features: potential dependent semicircle at high-frequency range which is associated to the charge transfer reactions, a Warburg type element at an angle of ~45° in the low-frequency region corresponds to diffusion of Li^+-ions and capacitive line at low frequency indicates the occupation of Li-ion in inserted sites [**26**]. **Fig. 4(a)** shows Nyquist plots related to the potential domain I, the potential applied from 0.5 to 0.65 V i.e. before de-

intercalation process begin. The main feature of this region is that it exhibits high-frequency semicircle (HFS) which is not complete towards the low frequencies [**26**]. The diameter of these arc-shaped curves slightly decreases with the increase in potentials followed by sloping, low-frequency capacitive line indicates the interfacial capacitance between the electrolyte and the electrode decreases with the applied potentials. Hence, this potential region I is dominated by capacitive behavior rather than de-intercalation process [**27**]. **Fig. 4(b)** related to potential domain II i.e. during de-intercalation measured from 0.84 to 0.90 V. The impedance measured between 0.84 to 0.90 V shows almost constant HFS near the cyclic voltammogram peak potentials, dominant Warburg at 45° angle and slight decrease in the capacitive line were observed which indicates favourable kinetic condition for lithium de-intercalation/intercalation rather than capacitive behaviour [**28**]. **Fig. 4(c)** covers the potential applied from 0.92 V to 1.0 V shows the end of Li-ion de-intercalation process (complete delithiated according to the CV potential domain III). In this potential domain III, the diameter of the HFS increases as the potential approaches towards the end of lithium de-intercalation and it shows the again increase in the capacitive line indicates the end of Li-ion de-intercalation process.

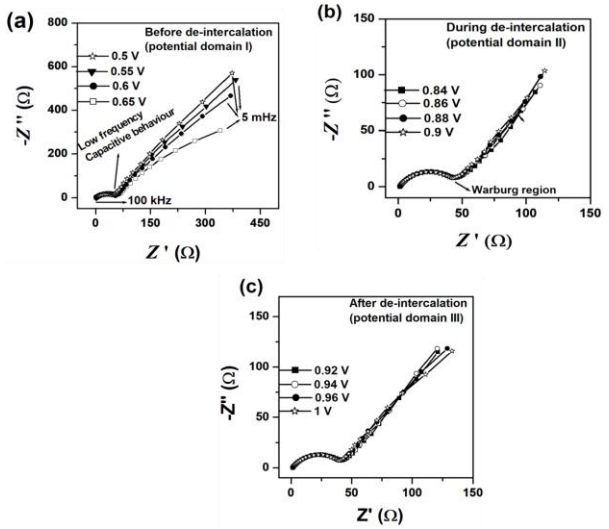

Fig. 4. Family of Nyquist plots for $LiVPO_4F/C$ in the aqueous electrolyte during the de-lithiated process. (a) before de-intercalation (b) during de-intercalation and (c) after de-intercalation.

Similarly, for the lithiated process of $LiVPO_4F/C$ was studied in the same manner as that of the de-intercalation process. The shape and magnitude of the Nyquist plots are similar to that of the de-lithiated process. **Fig. 5(a-c)** shows the typical Nyquist plots of $LiVPO_4F/C$ for intercalation process measured at different electrode potential range from of 1 to 0.5 V. **Fig. 5(a)** shows the Nyquist plots related to the potential domain I*****, in this domain I*****, the high-frequency semicircle (HFS) maintain constant but sloping capacitive line decreases as the potential approaches to CV peak potential [**28**]. Here in this domain, I*****, the beginning of Li-ion takes place from 1 to 0.85 V is as shown in **Fig. 5(a)**. **Fig. 5(b)** covers the impedance spectra of the electrode related to potential domain II* potential applied from 0.82 to 0.70 V and it is corresponding to the CV peak potential. In this potential domain, the low-frequency part of the spectra relates to the redox behavior of the $LiVPO_4F/C$ electrode and diffusion is the main process [**27**] which can be indicated by a slight decrease in the capacitive line and dominant Warburg behavior was observed that reflect the solid-state diffusion of Li-ions. The carbon residue in the triclinic $LiVPO_4F/C$ samples also enhances the lithium ion intercalation kinetics, which resulted in a smaller R_{CT} semicircle. Potential domain III*****, **Fig. 5(c)** covers the impedance spectra from 0.65 to 0.5 V shows the end of intercalation process. In this domain, the diameter of the semicircle is independent of the potential applied [**25**] and the low-frequency capacitive line becomes more pronounced and it shows line vertical to the Z' axis which corresponds to the capacitive line instead of the diffusion process. Hence, in this domain, the capacitive behavior is more prominent than the Warburg behavior.

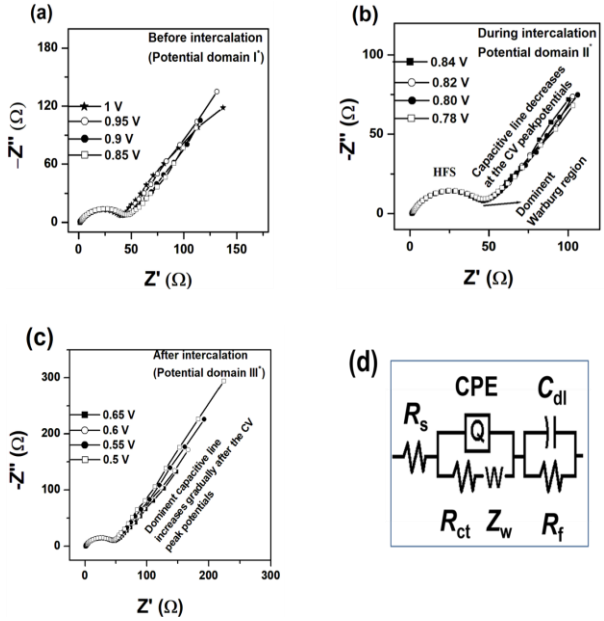

Fig. 5. Family of Nyquist plots for $LiVPO_4F/C$ during lithiation process (a) before intercalation (b) during intercalation and (c) after intercalation and (d) Equivalent circuit obtained during both de-intercalation/intercalation process (potential domain II/II*****).

The Nyquist plots, particularly in the potential domain II for both de-lithiated and lithiated process in the aqueous electrolyte are often interpreted using the electrical equivalent circuit as shown in **Fig. 5(d).** The obtained electrical equivalent circuit was found to provide the best fits for all Nyquist plots particularly to simulate the whole range of de-intercalation/ intercalation process. The kinetic parameters were obtained by simulation include R_s, R_{ct}, Z_w, CPE, R_f, and C_{dl}. R_s indicate the solution resistance; R_{ct} is related to charge-transfer between the surface film and solution.

Z_w corresponds to Warburg impedance for finite length diffusion in the bulk electrode and CPE is the constant phase element. R_f is the resistance for Li^+ migration through the surface film and C_{dl} represents double layer capacitance. The pure capacitor in the equivalent circuit is replaced by constant phase element (CPE). The CPE element replaces the capacitor due to a highly porous or roughness of the electrode surface [**29**]. The equivalent circuit consists of two RC circuits in series and the entire circuit components is classified into 3 component they are i) solution resistance and charge transfer resistance at higher frequency region ii) CPE indicates the presence of thin film layer on the electrode [**29**] and iii) Warburg element in low frequency region at a slope of 45°. Good fitting results were obtained for both de-intercalation/deintercalation processes.

From the equivalent circuit, the values of the kinetic parameters obtained for both de-lithiated/lithiated processes are displayed in **Table 1** and **2**. According to the data obtained in **Table 1** and **2**, R_s maintained almost constant, because solution composition and conductance do not change [**30**] throughout the applied potentials. R_{ct} values slightly decreased and reach a minimum near to the CV peak (potential domain II and II*****) as can be seen at 0.92 V for charge process and at 0.80 V for discharge process and steady increases after the CV peak was noticed and it is similar to reported articles [**28, 31**]. Evidently, Z_w shows maxima correspond to CV peak potentials and it is dominant at 0.92 and 0.82 V for de-intercalation/ intercalation process respectively. This can be explained on the basis of CV current, the current flow is poor or no change in the current before de-intercalation/intercalation process, whereas during the de-intercalation/intercalation process gradual increasing the current and it reaches a maxima/minima at the vicinity of the CV peak was observed and after the CV peak, the current gradually decreases. Correspondingly, C_{dl} values decrease as the potential increases and it is totally decreasing at the vicinity of the CV peak potential [**30**]. From the EIS spectra, the diffusion coefficient of lithium ions (D_{Li^+}) for de-intercalation/ intercalation process was calculated from the well-known equation [**30**].

$$D_{Li^+}=1/2[V_m(dE/dx)/nFAZ_w]^2 \quad (1)$$

where, V_m is the molar volume of $LiVPO_4F/C$ which is 5.2346×10^{-5} m^3 mol^{-1} [**31**], n is the number of electrons per molecule here n=1, dE/dX was calculated from the slope of the *x* value vs. potential [**27**], F is the Faraday constant (96,486 kJ), *A* is electrode surface area (0.5) and Z_w is the Warburg factor at a lower frequency. The variation of D_{Li^+} vs. potential (V) calculated by using **equation 1** is presented in table I and II. The D_{Li^+} vs. potential (V) plots decreases as the potential approaches to CV peak potentials and shows minima at 0.88 V for anodic process and 0.82 for cathodic process respectively which is related to CV peak potential.

Table 1. Evaluated impedance parameter according to the equivalent circuit of Fig. 5(D) as a function of electrode potential during the charging process.

E(V)	R_s (Ω)	R_{ct}(Ω)	Z_w(Ω)	C_{dl}(mF)	($D_{Li}/10^{-12}$) /cm^2s^{-1}
0.50	2.267	11.84	0.000127	0.590	3.5600
0.55	2.231	9.699	0.000133	0.527	3.3560
0.60	2.298	9.012	0.000138	0.518	1.7650
0.65	2.285	9.717	0.000140	0.5405	1.5990
0.70	2.287	9.084	0. 000274	0.5224	1.0678
0.75	2.236	0.579	0.004653	0.4427	0.8780
0.80	2.282	5.677	0.00196	0.4881	0.6990
0.84	2.225	12.22	0.00318	0.4831	0.4546
0.86	2.201	19.78	0.00325	0.290	0.1760
0.88	2.297	41.92	0.00392	0.141	0.0560
0.90	2.23	64.93	0.00954	0.098	0.0167
0.92	2.199	67.66	0.00084	0.6993	0.1569
0.94	2.23	67.89	0.00067	1.056	0.3560
0.96	2.235	74.77	0.000645	3.878	0.3610
1.0	2.30	105.88	0.000247	3.898	0.3460

Table 2. Evaluated impedance parameter according to the equivalent circuit of Fig 5(D) as a function of electrode potential during the discharge process.

E(V)	R s (Ω)	R ct(Ω)	Z w(Ω)	C dl(mF)	($D_{Li}/10^{-12}$) /cm^2s^{-1}
1.0	2.206	104.96	0.00013	3.805	1.9098
0.95	2.191	98.290	0.00047	0.4731	1. 3465
0.90	2.199	57.290	0.00047	0.4729	0.6676
0.88	2.225	33.532	0.00053	0.0249	0.4546
0.86	2.230	24.028	0.00357	0.0025	0.3807
0.84	2.205	19.517	0.00389	0.0046	0.1546
0.82	2.278	16.400	0.00532	0.0379	0.0865
0.80	2.310	35.800	0.00591	0.3180	0.0787
0.78	2.218	36.900	0.00570	0.4739	0 .9770
0.76	2.082	48.500	0.00015	0.3266	1.6780
0.70	2.293	75.680	0.00091	0.3775	2.7970
0.65	2.235	79.670	0.00016	0.4630	2.7680
0.60	2.250	105.60	0 .00013	0.9780	2.8850
0.55	2.356	105.780	0.00012	1.0448	2.9450
0.50	2.320	109.567	0.00010	1.9690	3.5770

Potentiostatic intermittent titration technique and galvanostatic intermittent titration technique

Electroanalytical methods such as PITT and GITT are the more superior and reliable techniques in the field of energy storage devices to determine the chemical diffusion coefficient of Li^+-ions [**32**]. The experiments performed were entirely based on CV incremental potential steps. PITT measurement was carried out for discharge process by applying small potential steps of 20 mV difference from 1 to 0.5 V and measured the current as a function of time. The resulting voltage and current data are plotted for the potential step of 0.81 V

is displayed in **Fig. 6(a)**. **Fig. 6(b)** shows the $It^{1/2}$ versus log *t* plot calculated from the same potential step of 0.80 V **[Fig. 6(a)]** and it describes the occurrence of different time domains. These different time domains are well evidenced in **Fig. 6(b)**, but in the case of **Fig. 6(a)**, the different time domains were overlapped in *I* versus *t* plot. According to the **Fig. 6(b)**, the progressive change in the shape of the chronoamperometric responses are indicated from letter A to F. the region A, indicates the interfacial charging of $LiVPO_4F/C$ cathode material and material/solution interfaces. Region B, indicated by lowest minima of $It^{1/2}$ which describes the semi-infinite planer diffusion. The plot basically shows a gradual decreasing in the slope with time and it shows a minimum in the region B indicates the Cottrell region i.e. pure diffusion of Li-ions in a short-time domain. This origin of the minima was theoretically explained by Montella [**33**]. The upward deviation of the plot after the Cottrell region at a longer time is due to the finite space diffusion in the $LiVPO_4F/C$ cathode and this region is represented by region D. Region C lies between the region B and D and it acts as a boundary between the short and long-time diffusions. Region E shows the intermediate stage which precedes the establishment of the new equilibrium. Finally, region F validate the establishment of new equilibrium state throughout the bulk of the electrode i.e. completion of the intercalation process. **Fig. 6 (c, d)** provides further evidence for the Li-ion intercalation and these plots were obtained from the *I* versus *t* plot. The experimental points deviate much from the tangent line which represents the pure diffusion-controlled process [**34**]. The behavior of variation of $It^{1/2}$ with log *t* plot indicated that the diffusion is not a single step in controlling the rate. This suggests the involvement of the ohmic resistance and slow finite-space diffusion in the lithium insertion process [**24**].

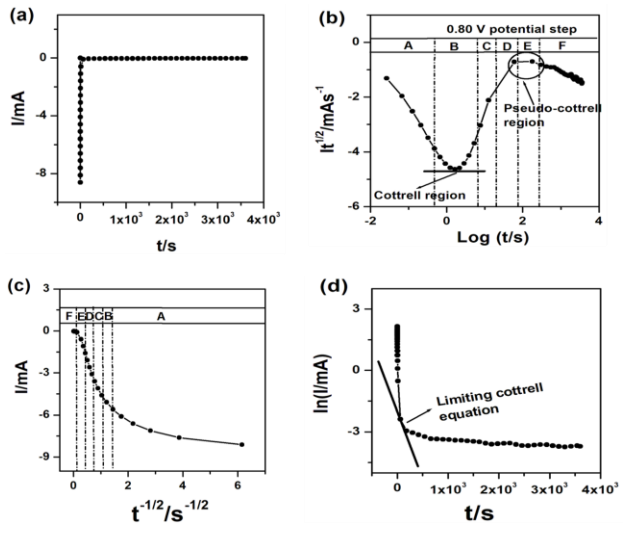

Fig. 6. (a) Typical chronoamperometric curve for $LiVPO_4F/C$ in the aqueous electrolyte during discharge process at 0.80 V potential steps. (b) $It^{1/2}$ vs. log *t* curve constructed from the data of Fig. 6(a) with separate kinetic regions marked by letters A to E. (c) I vs. $t^{1/2}$ (d) *t* vs. lnI plots calculated from the data of Fig. 6(a).

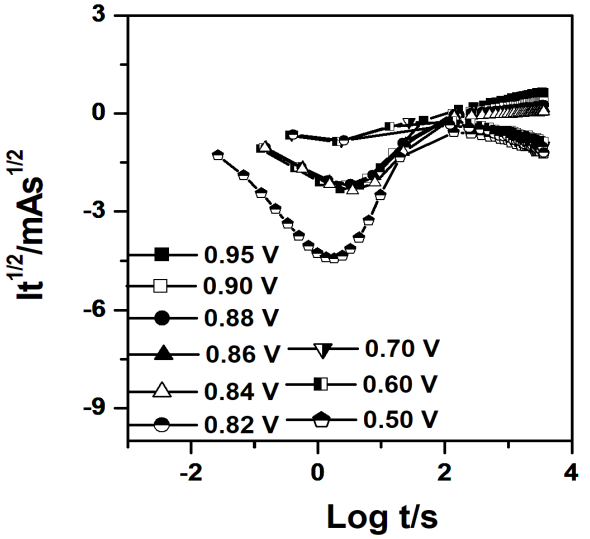

Fig. 7. $It^{1/2}$ vs. log t plots for different applied potential steps around the voltammetric peak during the discharge process.

Fig. 7 present the potential dependence of experimental $It^{1/2}$ vs. log *t* measured for whole intercalation process by applying small potential steps. All the $It^{1/2}$ vs. log *t* curves are similar to each other and exhibit similar characteristic feature with time quantitively at different potentials applied. The characteristic time constant corresponding to the Cottrell region also shows a peak like changes with highest $It^{1/2}$ at the vicinity of the CV peak i.e. the graph with the Cottrell region appearing at the shortest time is the one with highest $It^{1/2}$ value [**35**]. The lowest minima values of $It^{1/2}$ are observed at potentials 0.82 and 0.8 V which corresponds to the CV peak potentials. According to the CV behavior, before lithium insertion occurs, the faradaic current flow is minimal. As the electrode potentials approach CV peaks, the Cottrell region begins to appear at the lower time scale [**35-37**] which can be indicated by a plateau.

Conclusion

RAPET method was successfully used for the preparation of microcrystalline $LiVPO_4F/C$ and $LiTiPO_4F$ electrode materials. From this low-temperature scheme, the pure products were obtained as compared to many other synthetic approaches reported in the literature. The mechanism of the redox reaction of $LiVPO_4F/C$ in the aqueous electrolyte is very likely to be a lithium insertion similar to that of the non-aqueous electrolyte. Good cycling stability and rate capability were achieved in the presence of glycerin additive. Further, in order to confirm the Li-ion diffusion/extraction in/from $LiVPO_4F$ in 0.1M Li_2NO_3 with 0.05 mL glycerin aqueous electrolyte, we carried out EIS and PITT methods specifically to determine the variation of kinetic parameters at different potential domains and to determine the diffusion coefficient of Li-ions in $LiVPO_4F$.

Acknowledgments

The authors would like to acknowledge the financial support from the science and engineering Research board, Department of Science and Technology, New Delhi. We also thank Sri. A.V.S. Murthy, Honorary Secretary, Rashtreeya Sikshana Samithi Trust and Dr. Snehalata G Nadiger, Principal, NMKRV College for women, Bangalore for their continuous support and encouragement.

References

1. Barker, J.; Gover, R.K.B.; Burns, P.; Bryan, A.; Saidi, M.Y.; Swoyer, J.L.; *J. Electrochem. Soc.* **2005,** *152*, A1776. **DOI:** 10.1016/j.jpowsour.2005.03.126
2. Zheng, J.C; Zhang, B.; Yang, Z.H.; *J. Power Sources* **2012**, *202*, 380. **DOI:** 10.1016/j.jpowsour.2011.10.144
3. Rangaswamy, P.; Suresh, G.S.; Kittappa, M.M.; *J. Solid State Electrochem.* **2016,** *20*, 2619. **DOI:** 10.1007/s10008-016-3240-5
4. Li, Y.; Zhou, Z.; Gao, X.P.; Yan, J.; *J. Power Sources* **2006**, *160*, 633. **DOI:** 10.1016/j.jpowsour.2006.01.067
5. Barker, J.; Saidi, M.Y.; Swoyer, J.L.; *J. Electrochem. Soc.* **2003**, *150*, A1394. **DOI:** 10.1149/1.1609998
6. Lee S.; Sung Soo Park.; *J. Solid State Chem.* **2013**, *204*, 329. **DOI:** 10.1016/j.jssc.2013.06.003
7. Tarascon, J.M.; Recham, N.; Armand, M.; Chotard, J.N.; Baranda, P.; Walker, W.; Dupont, L.; *Chem. Mater.* **2010**, *22*, 724. **DOI:** 10.1021/cm9030478
8. Rangaswamy, P.; Suresh, G.S; Mahadevan, M.K.; *Chemistry Select*, **2016**, *1*, 1472. **DOI:** 10.1002/slct.201600388
9. Zhang, Q.; Zhong, S.; Liu, L.; Liu, J.; Jiang, J.; Wang, J.; Li, Y.; *J. Phys. Chem. Solids*, **2009**, *70*, 1080. **DOI:** 10.1016/j.jpcs.2009.06.001
10. Xiao, P.F.; Lai, M.O.; Lu, L.; *Solid State Ionics* **2013**, *242*, 10. **DOI:** 10.1016/j.ssi.2013.04.002
11. Kim, M.; Lee, S.; Kan, B.; *Adv. Sci.* **2016**, *3*, 1500366 **DOI:** 10.1002/advs.201500366
12. Ma, R.; Shao, L.; Wu, K.; Shui, M.; Wang, D.; Long, N.; Ren Y.; Shu, J.; *J. Power Sources* **2014**, *248*, 874. **DOI:** 10.1016/j.jpowsour.2013.10.029
13. Plashnitsa, L.S.; Kobayashi, E.; Okada, S.; Yamaki, J.I.; *Electrochim. Acta* **2011**, *56*, 1344. **DOI:** 10.1016/j.electacta.2010.10.051
14. Pol, V.G.; Pol, S.V.; Gedenken, A.; *J. Phy. Chem C* **2008**, *112*, 6627. **DOI:** 10.1021/jp711579n
15. Li, W.; Dahn, J.R.; Wainwright, D.S.; *Science*, **1994**, *264*, 1115. **DOI:** 10.1126/science.264.5162.1115
16. Wang, Y.; Yi, J.; Xia, Y.; *Adv. Energy Mater.*, **2012**, *2*, 830. **DOI:** 10.1002/aenm.201200065
17. Ruffo, R.; Wessells, C.; Huggins, R.A.; Cui, Y.; *Electrochem. Commun*. **2009**, *11*, 247. **DOI:** 10.1016/j.elecom.2008.11.015
18. Rangaswamy, P.; Suresh, G.S; Mahadevan, M.K.; Arthoba Nayaka, Y., *Chemistry Select*, **2018,** *3*, 3056. **DOI:** 10.1002/slct.201702132
19. Ouatani, L.E; Dedryvere, R.; Siret, C.; Biensan, P.; Gonbeau, D.; *J. Electrochem. Soc.* **2009**, *156*, A468. **DOI:** 10.1149/1.3111891
20. Shui Zhang, S.; *J. Power Sources*, **2006**, *162*, 1379. **DOI:** 10.1016/j.jpowsour.2006.07.074
21. Ateba Mba, J.M.; Masquelier, C.; Suard, E.; Croguennec, L.; *Chem. Mater.*, **2012**, *24*, 1223. **DOI:** 10.1021/cm3003996
22. Recham, N.; Chotard, J.N.; Jumas, J.C.; Laffont, L.; Armand, M.; Tarascon, J.M.; *Chem. Mater*., **2010**, *22*, 1142. **DOI:** 10.1021/cm9021497
23. Minakshi, M.; Pandey, A.; Blackford, M.; Ionescu, M.; *Energy Fuels*, **2010**, *24*, 6193. **DOI:** 10.1021/ef101063h
24. Liu, X.H.; Saito, T.; Doi, T.; Okada, S.; Yanaki, J.I.; *J. Power Sources*, **2009**, *189*, 706. **DOI:** 10.1016/j.jpowsour.2008.08.050
25. Zhang, Q.; Zhong, S.; Liu, L.; Liu, J.; Jiang, J.; Wang, J.; Li, Y.; *J. Phys. Chem. Solids* **2009**, *70*, 1080. **DOI:** 10.1016/j.jpcs.2009.06.001
26. Mahesh, K.C.; Manjunatha, H.; Venkatesha, T.V.; Suresh, G.S.; *J. Solid State Electrochem.* **2012**, *16*, 3011. **DOI:** 10.1007/s10008-012-1739-y
27. Manjunatha, H.; Mahesh, K.C.; Suresh, G.S.; Venkatesha, T.V., *Electrochim. Acta*, **2011**, *56*, 1439. **DOI:** 10.1016/j.electacta.2010.08.107
28. Mahesh, K.C.; Suresh, G.S.; Venkatesha, T.V.; *J. Solid State Electrochem.*, **2012**, *16*, 3559. **DOI:** 10.1007/s10008-012-1787-3
29. Ho, C.; Raistrick, I. D.; Huggins, R. A.; *J. Electrochem. Soc*., **1980**, *127*, 343. **DOI:** 10.1149/1.2129668
30. Wang, G.J.; Qu, Q.T.; Wang, B.; Shi, Y.; Tian, S.; Wu, Y.P.; Holze, R.; *Electrochim. Acta*, **2009**, *54*, 1199. **DOI:** 10.1016/j.electacta.2008.08.047
31. Shivashankaraiah, R.B.; Manjunatha, H.; Mahesh, K.C.; Suresh, G.S.; Venkatesha, T.V.; *J. Solid State Electrochem*, **2012**, *16*, 1279. **DOI:** 10.1007/s10008-011-1520-7

32 Levi, M.D.; Gamolsky, K.; Aurbach, D.; Heider, U.; Oesten, R.; *J. Electroanal. Chem.* **1992**, *477*, 32. **DOI:** 10.1016/S0022-0728(99)00386-1

33. Montella, C., *J. Electroanal. Chem.* **2002**, *518*, 61. **DOI:** 10.1016/S0022-0728(01)00691-X
34. Manjunatha, H.; Mahesh, K.C.; Suresh, G.S.; Venkatesha, T.V., *Electrochim. Acta* **2012**, *80*, 269. **DOI:** 10.1016/j.electacta.2012.07.003

35. Xiao, P.F.; Lai, M.O.; Lu, L., *Solid State Ionics* **2013**, *242*, 10. **DOI:** 10.1016/j.ssi.2013.04.002

36. Levi, M.D.; Levi, E.A.; Aurbach, D.; J. *Electroanal. Chem.* **1997**, *421*, 89. **DOI:** 10.1016/S0022-0728(96)04833-4
37. Levi, M.D.; Markevich, E.; Aurbach, D.; *J. Phys. Chem. B* **2005**, *109*, 7420. **DOI:** 10.1021/jp0441902

